U. of Colorado
95626
Final Report

9950-1091

14 April 84 SDO/SWG Draft Toomre/Hill/Merryfield/Gough Chapter 4

B. THE PROBLEM OF ATMOSPHERIC TURBULENCE

This report was prepared for the Jet Propulsion Laboratory, California Institute of Technology, sponsored by the National Aeronautics and Space Administration.

B. THE PROBLEM OF ATMOSPHERIC TURBULENCE

All ground-based observations of the solar five-minute oscillations are affected by turbulence in the Earth's atmosphere that leads to substantial refractive index variations. The turbulent motions serve to mix an air mass that is thermally stratified in the vertical, thereby producing intermittent thermal fluctuations over a wide range of heights in the atmosphere. These thermal structures yield refractive index changes that deflect the light path in a complicated way, producing intricate variations of amplitude and phase in what might have started out as simple plane waves. Since the fluid turbulence is statistical in nature, so too is the optical turbulence which is an integral measure of the refractive index changes along the light travel path. All of this produces what is usually called "atmospheric seeing", which consists of image motion, blurring and distortion across the field of view.

We will begin to assess here the effects of atmospheric seeing upon observations of five-minute oscillations carried out from the ground. This will help to provide a baseline estimate of the scientific benefits that might accrue if one were able to observe the same oscillations from a space observatory unfettered by seeing effects. Such an assessment is however not a simple undertaking, for there are wide variations in the seeing experienced at a given observing site, and there are equally great changes between different sites. But more importantly, seeing produces image distortions that are often truly nonlinear in character, with light travel paths crossing and even focusing onto caustics. Further, the reliable modelling of atmospheric seeing shares the intrinsic difficulties of turbulence theory itself, for both depend critically upon understanding and describing the highly nonlinear dynamics of the atmosphere.

1. Numerical Simulations of Impact of Atmospheric Turbulence

Our assessment here of the effects of seeing will be based on extensive numerical simulations that we have carried out in which solar oscillations are viewed through a distorting atmosphere that is varying in both space and time. The simulations have dealt in turn with both high ℓ and intermediate ℓ modes of oscillation, for we expect these to be more gravely influenced by atmospheric seeing than the low degree modes. Our numerical simulations have involved: a) Constructing synthetic velocity data set that represent the superposition of many oscillation modes as they may appear on the surface of the Sun. b) Observing such oscillations through a distorting atmosphere that serves to deflect the light paths in a stochastic manner across the field of view. c) Reducing the observations with Fourier transforms to obtain (ℓ,ν) power diagrams, and then evaluating how the signal-to-noise ratio in the transforms varies with the quality of the seeing. We now turn to discuss in more detail these three elements of the numerical simulations, and then present the results.

a) Simulated Velocity Fields for Oscillations and Steady Flows

We have constructed synthetic Doppler velocity data sets involving two spatial dimensions and time that would result on the Sun if about 100 modes of oscillation (with distinctive frequencies ν and spherical degrees ℓ) were superimposed upon a persistent background velocity field attributable to supergranulation and mesogranulation. Although of order 10^6 modes of oscillation are actually superimposed on the real Sun, our 100 or so modes will serve to sample a fairly broad range of ν and ℓ and thus identify which modes are affected most severely by the seeing. Thus in our high ℓ simulations we will choose oscillation modes that serve to populate the p_1 and

p_2 ridges in power and span ℓ values from 150 to 450 in increments of 6. In the corresponding intermediate degree simulations, the ℓ values for the sampling modes range from about 50 to 150.

As sketched in Figure 4.B.1, the Doppler velocities (with suitable geometric projection taken into account) are evaluated for each time interval on a regular two-dimensional spatial grid composed of 256 × 32 elements or pixels in the plane of the sky, with each pixel covering an area of 7" × 7". Such a relatively long but narrow sampling window, covering much of the solar diameter along the equator, is appropriate for observing oscillation modes (with azimuthal order m equal to spherical degree ℓ) that can probe the dynamics of giant cells and of differential rotation in the convection zone. The Doppler velocities are evaluated over the spatial sampling window for 512 successive time intervals, each separated by 60 seconds in time from the former so that the oscillations (ranging in period from about 200 to 400 seconds) can be suitably sampled in time. Each simulation thus spans about 8.5 hours in time, which is comparable to what is typically achievable on a given day from a mid-latitude ground observatory.

b) Modelling the Seeing Distortion

The atmospheric turbulence will lead to differential image motion, blurring and distortion across the field of view in the sky. Theory and experiment concerning such optical turbulence has led to a broad and competent literature which seeks to explain the spectral characteristics of the atmospheric seeing and its impact on astronomical observations (e.g. Refs. 1-12). We shall not review here the details of the modulation transfer functions, index-of-refraction structure parameters, or transverse coherence lengths that are the necessary tools of that subject. Rather, we will turn directly to their predictions of typical image displacements that can be

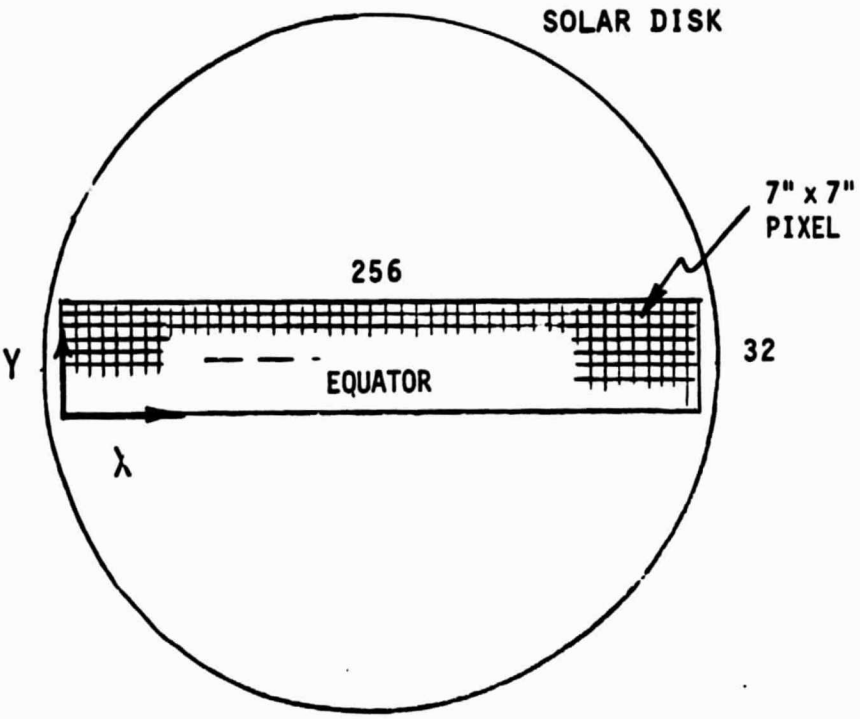

Figure 4.B.1 Sampling grid of 256 × 32 pixels on the solar disk used in simulation of atmospheric seeing effects on observation of solar oscillations.

expected, with these expressed as Fourier spectra in the temporal and spatial frequency domains.

We will simulate the effects of seeing by evaluating at any given instant in time an array of image displacements across the field of view. The Doppler velocities as previously calculated on the solar disk are then "observed" through such a seeing displacement matrix. This serves to displace each image element in a particular spatial direction by a specified fraction or multiple of a pixel. The observed Doppler velocity field at a given pixel may thus involve fractional contributions from many nearby pixels.

The instantaneous two-dimensional image displacement arrays are constructed by inverse Fourier transforms of a two-dimensional spatial power spectrum that possesses a Kolmogorov $k_h^{-5/3}$ decrease at high horizontal wavenumbers k_h, preceded by a relatively flat plateau between a range of lower wavenumbers. The plateau at low k_h corresponds to the large scales of turbulence that are dynamically driven; a turbulent cascade of energy to higher wavenumbers produces the Kolmogorov inertial range. Accurate telescope guiding is assumed to compensate for the seeing displacements of very large spatial scale (or small k_h), and consequently the power in the transforms is assumed to vanish as k_h goes to zero. The power spectrum has added to it proportional Gaussian noise at all wavenumbers; the specified phases for the transforms are obtained from uniformly distributed noise. We can consider a variety of seeing conditions by varying the upper and lower cutoff wavenumbers for the plateau in the power spectrum. For convenience, we will here generally specify the quality of the seeing by just referring to the rms average spatial displacement that results from a given class of these power spectra.

The seeing displacements vary rapidly in time compared to our once per 60 second sampling of the Doppler velocities. As in the spatial domain, the

representative temporal power spectrum of seeing displacements possesses a plateau followed by a Kolmogorov decrease with increasing frequency. Since the transition is already achieved at periods of only a few seconds, seeing displacement arrays separated in time by more than about 5 seconds would show almost no correlation. We have exploited this property in our simulations by constructing a large number (64 or greater) of spatial displacement arrays, and then proceeding to randomly select one of these to apply the seeing displacements at any given instant in time. We further can estimate the benefits of long exposures by applying a sequence of image displacements to a given velocity realization.

Our simulations in many ways represent optimal estimates of what can be done from the ground, for we have omitted all explicit effects of noise introduced by instrumentation to measure the Doppler signal, and have not concerned ourselves with how fluctuations in the transmission of intensities in the atmosphere would influence the determination of Doppler velocities from spectral lines. These are all quite subtle issues that depend in detail upon the Doppler analyzer that is being used.

c) Analyzing the Observations

The velocity fields that have been subjected to seeing distortions are then analyzed to determine how the power in the oscillations may have been redistributed in both frequency and wavenumber. Any given data set consists of 512 time samples of 256 × 32 spatial arrays. In order to isolate those oscillation modes that travel along the equator from other signals, we will suitably average the Doppler velocities in the shorter spatial dimension (shown as y in Figure 4.B.1), thereby obtaining a data array in the remaining spatial dimension (x) and in time (t). Such an array is then Fourier transformed to obtain two-dimensional power spectra in horizontal wavenumber

k_h (or spherical degree ℓ) and frequency ν. Detailed comparison will be made of power spectra obtained with different qualities of seeing.

2. Results of Seeing Simulations

The power spectra of the solar oscillations are influenced both by effects of geometry when viewing a sphere from a single vantage point and by effects of atmospheric seeing. We begin by illustrating in Figure 4.B.2 the geometrical effects alone. Panel (a) there shows the power spectrum that would result if the velocity fields of the high ℓ oscillations could have been observed equally well at all longitudes ϕ over the portion of the sphere under study. However, as viewed in projection on the plane of the sky, the wave fronts near the limb would appear much closer together than those at disk center. Panel (b) shows the power spectrum that is obtained if the spatial transforms were simply carried out over the uniformly-spaced grid in x that forms the longer dimension of our sampling window in Figure 4.B.1. Thus ignoring the spatial foreshortening toward the limb leads to a sharp decrease in power in both the p_1 and p_2 ridges and high noise levels in between. Panel (c) shows what can be achieved if we correct for the foreshortening by interpolating the data in x onto a uniform grid in ϕ and then carrying out the transform. The ridges in power have reasserted themselves, though the power levels at the higher ℓ values are diminished. Such shifting of power away from the ridges and toward higher ℓ, leading to the shadow bands seen to the right in panel (c), is just the consequence of undersampling the wave fronts close to the limb when using a uniform sampling grid. Not surprisingly, specifying the spatial pixel size (here 7" × 7") controls the highest ℓ that can be detected, but the decrease in sensitivity is gradual and power is redistributed in some uncanny ways.

We turn now to the effects of atmospheric turbulence superposed on those of geometry. All the data have been analyzed with foreshortening corrected in the manner of the previous Figure 4.B.2c, and the power levels displayed with identical scaling to aid the comparison. Degrading the seeing quality when observing the high ℓ oscillations leads to the results presented for 2" and 3" rms seeing displacements in Figure 4.B.3 and for 4" and 5" seeing in the companion Figure 4.B.4. The power spectra shown in the upper panels (a) are based on short exposures in time per Doppler measurement; here the steady background velocity fields of supergranulation (SG) have been omitted. In contrast, the spectra shown in the middle panels (b) include the effects of those persistent velocities. Finally, the spectra in the lower panels (c) display the benefits of using long exposures per measurement of the combined oscillatory and steady velocities. The 2" seeing shown in (a) has little effect on the ridge structures, whereas 3" seeing has already diminished the power levels in the ridges at the higher ℓ values. This tendency is accentuated with 4" seeing, and 5" seeing yields very feeble and severely shortened ridges. The inclusion of the supergranular velocity fields has an effect that is increasingly dramatic as the seeing degrades. Whereas the power spectrum in panel (b) with 2" seeing and a short exposure just shows a mild increase in the noise level between the ridges, the adjacent panel with 3" seeing shows a prominent increase in the choppy background of power. Going to the companion spectra with 4" seeing shows that the ridges in power are almost becoming obliterated by the background, as they indeed are with 5" seeing. The longer exposures in panels (c) that average over 4 seeing realizations per Doppler measurement help to diminish the background choppiness, yielding ridges that are now somewhat discernible with 4" seeing but not usefully so with 5" seeing.

These seeing simulations of high ℓ oscillations, with ℓ ranging from 150 to 450, reveal that atmospheric turbulence can severely degrade the Doppler velocity data, and clearly the higher ℓ values are affected the most seriously. The signal-to-noise ratio in these (ℓ,ν) power spectra is influenced by seeing in two ways. Firstly, seeing distortions of the oscillation wave fronts cause some of the power to be moved away from their appropriate (ℓ,ν) values. This process is more vigorous for oscillations with the shorter horizontal wavelengths (or greater ℓ values). Thus the ridges in power are preferentially obliterated at their high ℓ values. Yet as damaging is that random image displacements convert steady velocity signals from the strong supergranular flows into apparently time-varying signals. Therefore power is partially redistributed from what should be zero frequency to a broad range of frequencies, causing the prominent noisy background that appears in the power spectra as the seeing gets worse. The impact of the atmospheric turbulence is thus twofold: not only do the ridges shrink in height, but the background due to persistent flows also rises up to further decrease the signal-to-noise ratio. It is this ratio which is critical to all of the applications of inverse theory to deduce the interior dynamics and structure. Namely, a wide selection of frequencies for the oscillation modes must be measured as precisely as possible, and the accuracy of such determinations depends sensitively on how well the power attributable to the oscillations can be isolated from the background. Using long exposures helps to somewhat mitigate the effects from supergranulation, but with 4" seeing there is little useful oscillatory signal left for ℓ values greater than about 300. Further, at ℓ values around 200, the signal-to-noise ratio in both the p_1 and p_2 ridges typically decreases by about a factor 3 in going from 2" to 3" seeing, and a further factor of about 3 in going to 4" seeing. With 5" seeing there is little signal left at $\ell = 200$ that survives over the background.

We estimate that what we designate as 2" seeing corresponds to pristine seeing conditions rarely encountered at most observatories, while 3" seeing is more typical of a day of consistently good seeing, and 4" seeing represents the worsening conditions that are often encountered under turbulent conditions. These numbers are not intended to be absolute, for we can adjust the plateau in the original input power spectra for the image displacements and thus somewhat worsen or improve the final (ℓ, ν) power diagrams shown here. However, the changes are systematic and gradual across the matrix of seeing that we have sampled, and thus we have chosen parameters for the illustrations here that appear fairly representative of atmospheric conditions.

The seeing simulations with intermediate ℓ oscillations, with ℓ ranging from 48 to 150, are presented in Figure 4.B.5. These oscillation modes with large horizontal wavelengths are not badly affected by the seeing until the seeing deteriorates to rms image displacements of about 4" or 5". These two seeing conditions are displayed in Figure 4.B.5, using a layout similar to the earlier figures except that the range of displayed frequencies ν and spherical degrees ℓ now both extend to zero values. The upper panels (a) again present power spectra obtained with short exposures while omitting supergranulation, while those in (b) include effects of persistent velocities which yield a very noisy background. Going to longer exposures in (c) serves to reduce that background somewhat. The jagged structures in power at $\nu = 0$ in panels (b) and (c) show the distribution with ℓ of power in the persistent velocities (after averaging across the shorter dimension y of the observing window). The noisy background at other frequencies reflects the range in ℓ present in such supergranulation. From these intermediate degree simulations we conclude that the signal-to-noise ratio in the vicinity of $\ell = 100$ is about a factor 3 worse with 4" seeing than it is with 2" seeing, while that ratio at $\ell = 50$ is only slightly affected by the range of seeing conditions considered here.

3. Conclusions from Seeing Simulations

We can conclude from these numerical simulations that the distribution of power along the ridges is influenced both by viewing a portion of a spherical surface from a single vantage point, and especially by the distortions of that view by atmospheric turbulence. The signal-to-noise ratio in the resulting observations of oscillations will deteriorate rapidly with increasing values of ℓ as the seeing worsens. What we have here sampled of intermediate ℓ modes shows that the power at $\ell = 50$ is little affected by the seeing, whereas that at $\ell = 100$ has a factor 3 deterioration in signal-to-noise ratio when the seeing involves 4" rms image displacements, as contrasted to pristine conditions. However when considering the high ℓ modes, 3" seeing already has a noticeable effect on that ratio at $\ell = 200$, while the more extreme 5" seeing has largely obliterated all information about those oscillations. At higher values of ℓ, the seeing must be correspondingly better to be able to make useful deductions from the frequencies of the oscillations.

It would be desirable to try to use such seeing simulations to estimate what is lost in the potential scientific content of the oscillation data due to seeing distortions. On the basis of our work so far, we cannot yet place specific limits on what could be deduced for instance about the internal rotational velocities of the Sun with depth and latitude. To do so would require a far more elaborate set of simulations combined with inversion of the data. Namely, one would need to carry out of order seven steps, of which we have here reported on the central four:

1) Invent for instance a functional form for the internal rotation curve, and from it construct appropriately shifted frequencies for the sampling modes.
2) Load the (x,y,t) simulation grid with Doppler oscillation data, using of order 1000 or so modes to allow for mode beating effects.

3) Superpose a background persistent velocity field on that of oscillations.
4) Observe that data set in (x,y,t) through various atmospheric distortion models in order to assess the effects of seeing.
5) Reduce the observations to (ℓ,ν) power diagrams.
6) Determine apparent frequencies for about 200 specific modes, and then analyze the results with inversion procedures to obtain estimates of the internal rotation.
7) Compare the deductions from inverse theory with the rotation law that went in at step 1, and determine how it varies with different seeing.

Our work so far has dealt mainly with steps 2 through 5, and has used fewer modes than would probably be needed for the inversion work. Clearly, detailed scientific assessments of the effects of seeing upon specific questions about internal dynamics and structure will require the application of inversion methods to suitably chosen oscillation data. Inversion methods by design make partial compensation for inconsistencies in the data that are introduced by noise of various kinds. Here we have determined how some of that noise comes about from the atmospheric turbulence, and have seen how that noise increases with ℓ as the seeing degrades. Even inversion methods are of little use when noise dominates signal, and the simulations here indicate which ℓ values become inaccessible due to the seeing distortions.

References

Barletti, R., Ceppatelli, G., Paterno, L., Righini, A., and Speroni, N. 1976, "Mean vertical profile of atmospheric turbulence relevant for astronomical seeing", J. Opt. Soc. Am., 66, 1380-1383.

Brandt, P. N. 1969, "Frequency spectra of solar image motion", Solar Phys., 7, 187-203.

Coulman, C. E., and Hall, D. N. B. 1967, "Optical effects of thermal structure in the lower atmosphere", Appl. Optics, 6, 497-503.

Endler, F., and Deubner, F. -L. 1983, "The influence of seeing on the observation of short period fluctuations in the solar atmosphere", Astron. Astrophys., 121, 291-296.

Forbes, F. 1982, "Dome induced image motion", SPIE Vol. 332 Advanced Technology Optical Telescopes, 185-192.

Fossat, E., Grec, G., and Harvey, J. W. 1981, "Power spectrum of differential refraction and comparison with solar diameter fluctuation measurements", Astron. Astrophys., 94, 95-99.

Fried, D. L. 1975, "Differential angle of arrival: Theory, evaluation, and measurement feasibility", Radio Sci., 10, 71-76.

Lawrence, R. S. 1976, "A review of the optical effects of the clear turbulent atmosphere", SPIE Vol. 75 Imaging through the Atmosphere, 2-8.

Roddier, F. 1981, "The effects of atmospheric turbulence in optical astronomy", Progr. Optics, 19, 281-376.

Walters, D. L. 1981, "Atmospheric modulation transfer function for desert and mountain locations: r_0 measurements", J. Opt. Soc. Am., 71, 406-409.

Walters, D. L., and Kunkel, K. E. 1981, "Atmospheric modulation transfer function for desert and mountain locations: the atmospheric effects on r_0", J. Opt. Soc. Am., 71, 397-405.

Young, A. T. 1974, "Seeing: Its cause and cure", Astrophys. J., 199, 587-604.

Figure Captions

Figure 4.B.2 Effects of geometry and a finite observing window upon observing high ℓ oscillation modes possessing spherical degrees ℓ ranging from 150 to 450 and frequencies ν corresponding to p_1 and p_2. Shown are power spectra in perspective views as functions of ℓ and ν.

Figure 4.B.3 Effects of image distortions arising from atmospheric turbulence upon observations of high ℓ oscillation modes. Panels (a) show power spectra of oscillations observed through seeing models possessing typical rms spatial displacements of 2" and 3". Panels (b) superpose persistent velocity fields of supergranulation (SG) upon those of the oscillations and then observe the combined Doppler velocities under both 2" and 3" seeing conditions. Panels (c) show power spectra in which the background noise is decreased by having used long exposures for each measurement of velocities.

Figure 4.B.4 As in Figure 4.B.4, but now considering how 4" and 5" seeing conditions have changed the power spectra of the high ℓ oscillations.

Figure 4.B.5 As in Figure 4.B.4, but showing power spectra for the intermediate ℓ simulations using modes p_1 and p_2 with ℓ values ranging from 48 to 150. Here effects of 4" and 5" seeing conditions are displayed.

HIGH ℓ OSCILLATION INPUT SPECTRA

a.

TRANSFORM ON
LONGITUDE ϕ-GRID

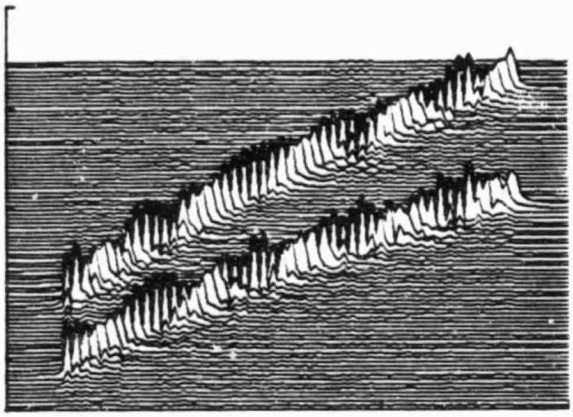

b.

TRANSFORM ON
PLANE-IN-SKY X-GRID

FORESHORTENING
NOT CORRECTED

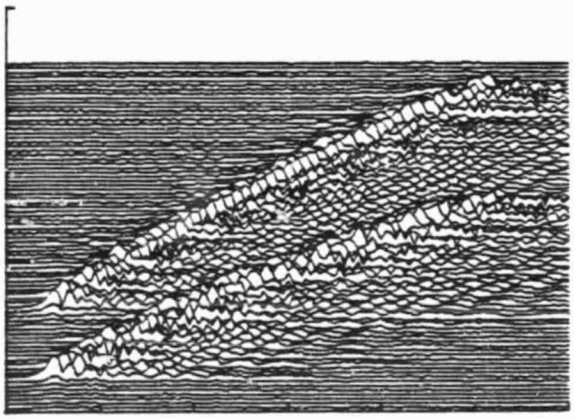

c.

TRANSFORM ON
X-GRID

FORESHORTENING
CORRECTED

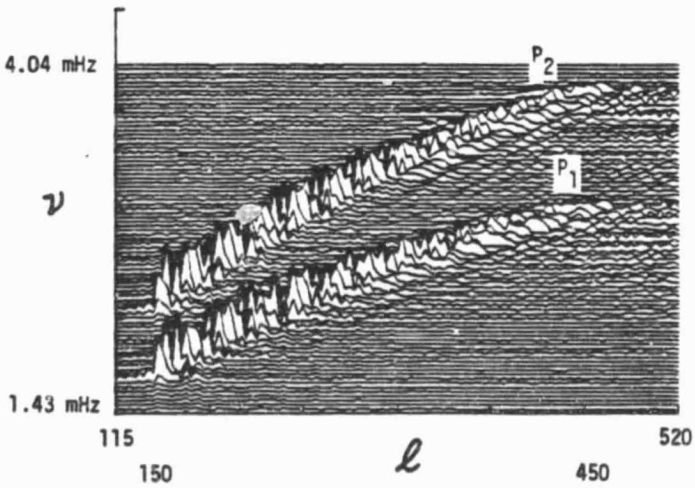

Figure 4.B.2

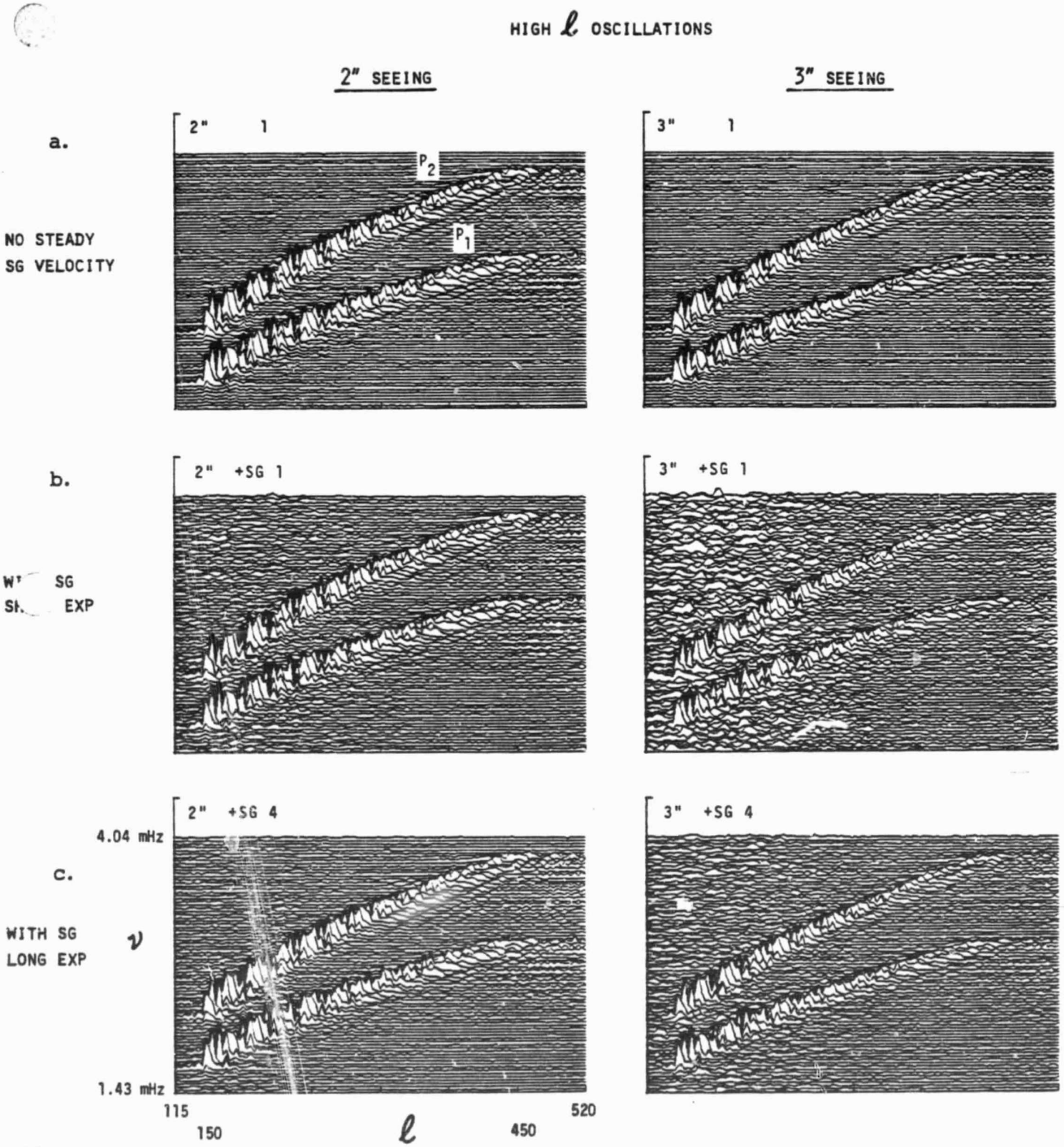
HIGH ℓ OSCILLATIONS
2" SEEING
3" SEEING
a.
NO STEADY
SG VELOCITY
2" 1
P2
P1
3" 1
b.
W' SG
Sl. EXP
2" +SG 1
3" +SG 1
c.
WITH SG
LONG EXP
2" +SG 4
3" +SG 4
4.04 mHz
1.43 mHz
ν
115
150
ℓ
450
520

Figure 4.B.3

HIGH ℓ OSCILLATIONS

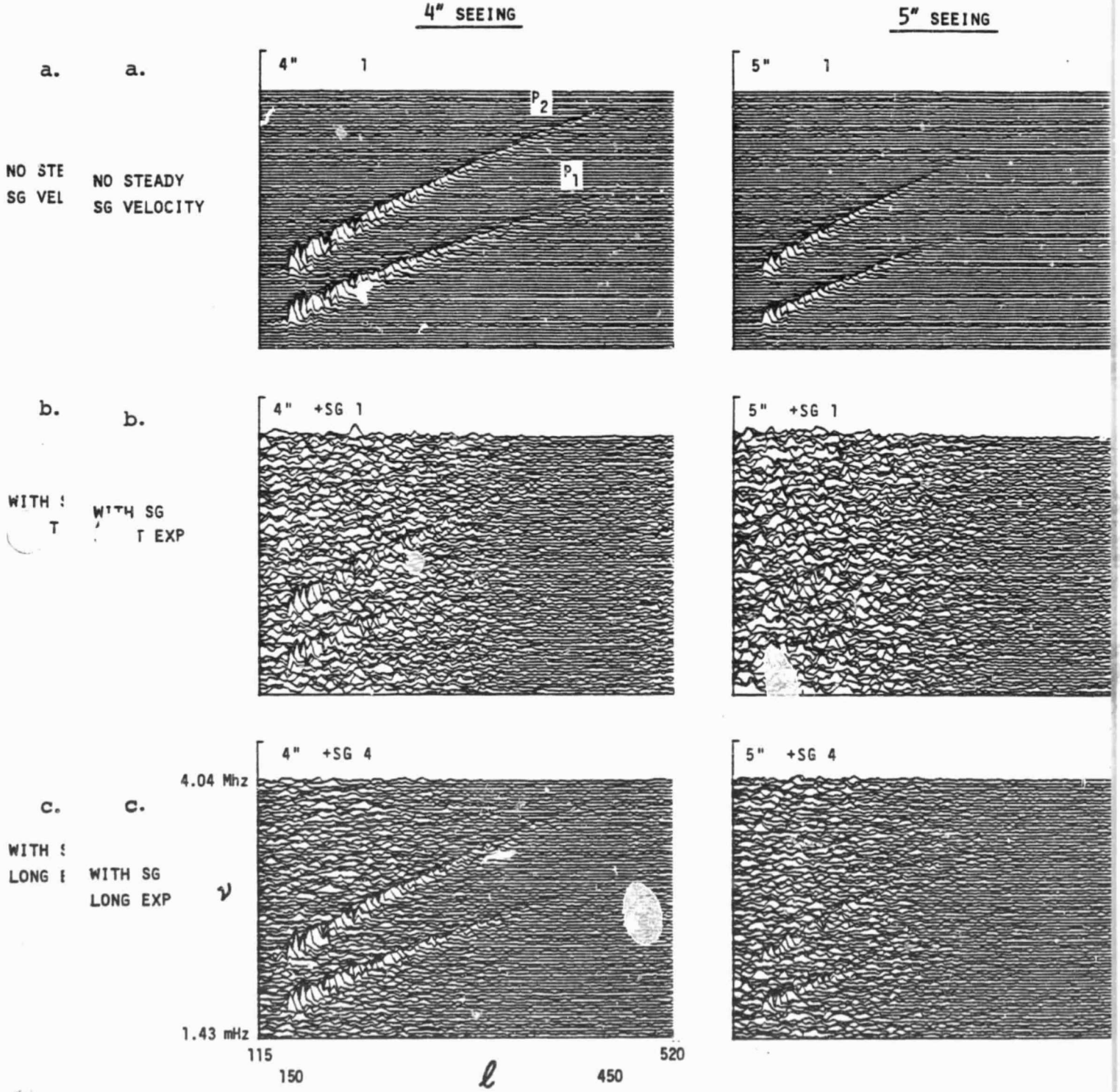

Figure 4.B.4

As appeared in final report

Chapter 4
The Limitations of Ground-Based Observations of Solar Oscillations

Space experiments, such as the one we advocate in this document, are expensive and require a long lead time. Their justification lies of course in the scientific achievements that they will make possible. In the case of helioseismology, the anticipated achievements build upon the very substantial success of ground-based studies. While these studies may be expected to make additional very important contributions over the coming years, observations from the ground face formidable limitations introduced by the atmosphere of the Earth and by the day-night cycle or gaps due to weather at individual observatories. In this chapter we explore these limits on ground-based capabilities and describe their impact on the scientific knowledge ultimately attainable from the ground.

A. The Problem of Atmospheric Turbulence

All ground-based observations of the solar oscillations are affected by turbulence in the Earth's atmosphere. This produces the phenomenon of "atmospheric seeing" that consists of image motion, blurring, and distortion across the field of view. Atmospheric seeing smears out the velocity field, reducing the measured power for spatial scales comparable to the smearing function. It also shifts the measured power into incorrect temporal frequencies and horizontal wave numbers, reducing the power where the signal is large and introducing spurious broadband power at other wave numbers and frequencies. These effects are particularly important for modes of high degree.

We have attempted to assess the effects of atmospheric seeing upon observations of solar oscillations carried out from the ground in two ways: by numerical simulations and by using the observational data in which solar oscillation time strings have been obtained with spatial resolution in two dimensions. Both assessments are described below.

1. Numerical Simulations of Atmospheric Turbulence Effects

In our numerical assessment of the effects of seeing, we have made extensive simulations of solar oscillations as viewed through a distorting atmosphere that varies in both space and time. This study is reported in detail in Appendix A; here we summarize the study and our conclusions from it.

The simulation study consisted of four parts:

(1) Constructing synthetic two-dimensional velocity fields $v(x, y, t)$ resulting from superposition of about 100 oscillation modes of intermediate degree ($\ell < 150$) and high degree ($150 < \ell < 450$). Also included was an appropriate background velocity field simulating the known properties of supergranulation and mesogranulation. This background velocity field is important, for its spatial gradients are so large that seeing-induced image displacements can introduce large spurious velocity fluctuations into the data.

(2) Simulating the effects of seeing by introducing a seeing-displacement matrix that displaced each image element of the velocity array in a random direction and by a random amount correlated with the quality of seeing chosen for the simulation. These displacements were derived from models of atmospheric turbulence.

(3) "Observing" the seeing-degraded velocity field while neglecting additional sources of noise such as instrumental noise, transparency variations, etc. Thus the "observation" represents an optimistic approximation to a real observation. Each simulated "observation" spanned about 8.5 hours (comparable to what can be obtained in one day at a typical ground-based observatory) with observations at 1-min intervals.

(4) Analyzing the "observation" to obtain power spectra in horizontal wave number k_h or degree ℓ and frequency ν.

As detailed in Appendix A, our seeing simulations employed in effect a "detector" of 256 × 256 spatial elements, with each pixel subtending an area 7 arcsec square on the Sun. Such a choice of pixel size was dictated by the need to span nearly the full solar diameter in the course of potential studies of the interior dynamics. To obtain information on modes of degree as high as $\ell \sim 600$, actual detectors must be as large as 1024 elements on a side, with pixels subtending an area 2 arcsec square. It was not computationally practical in these already elaborate numerical simulations to deal with such large data arrays. However, as we shall see immediately below, it is already clear from the present simulations that seeing effects lead to drastic diminution in apparent power at typical ℓ values of about 300 or greater when the seeing is less than excellent. The use of smaller sampling pixels cannot cure that trend, even though at times of exceptional seeing conditions the use of such small pixels would allow one to see ridge structures at ℓ values as high as $\ell \sim 600$. Even then, the power there is severely attenuated by the seeing effects, and the signal-to-noise ratio is marginal for inverting the data.

Simulations were performed with different qualities of simulated seeing so that one may compare how the signal-to-noise ratio in the "observed" ℓ-ν diagrams depend on the quality of the seeing. Some of the results are illustrated in Fig. 4-1.

In Fig. 4-1(a) we see that for intermediate ℓ oscillations ($\ell < 150$) the seeing is not a serious problem even for 4-arcsec seeing (a typical "average" seeing level at midday at a good solar site). However, as shown in Fig. 4-1(b), for higher ℓ oscillations, the problem becomes increasingly severe so that the oscillation signal for $\ell \geq 200$ become seriously degraded when the seeing quality deteriorates below about 3 arcsec. We note that 3-arcsec seeing is better than average for a many-hour observing run at most observatories.

We conclude from these numerical simulations that the distribution of power along the ridges is strongly influenced by atmospheric turbulence. The signal-to-noise ratio in the resulting observations will deteriorate rapidly with increasing values of ℓ as the seeing worsens. Our sampling of intermediate ℓ modes shows that the power at $\ell = 50$ is little affected by the seeing, while that at $\ell = 100$ deteriorates by a factor of 3 in the signal-to-noise ratio when the seeing involves 4-arcsec rms image displacements, as contrasted to pristine conditions. For $\ell = 200$, even 3-arcsec seeing has a noticeable effect on the signal-to-noise ratio, while 5-arcsec seeing has largely obliterated all information about the oscillations. At still higher values of ℓ, the seeing must be correspondingly better in order to make useful deductions from the frequencies of the oscillations.

From this simulation (and actual experience using ground-based detection systems, as described below), it thus appears that there is a natural breakpoint between what can practically be observed on a regular basis through the turbulent atmosphere and what cannot. This deterioration begins, roughly speaking, at $\ell \sim 200$. Of course, the deterioration with increasing ℓ is not sharp. Oscillations with relatively high amplitude (e.g., those in the 5-minute region) should be observable with good signal-to-noise ratio to considerably higher ℓ values than those of low amplitude.

2. Observational Confirmation of the Deleterious Effects of Seeing

The predicted effects of seeing are (1) that the observed power at high ℓ values should be reduced under conditions of poor seeing relative to times of good seeing and (2) that the observed power for combinations of frequency and wavelength where the solar power is small should be increased during periods of poor seeing relative to periods of good seeing. To test these two predictions, we have analyzed a 9.1-hour (all day) run of oscillation data by breaking it into two equal subsets, the first reflecting morning conditions and the second afternoon conditions. The observations were obtained at Mt. Wilson Observatory, where the morning seeing is almost always superior to the afternoon seeing. The data consist of velocity images obtained with the resonance line filter described in Appendix F. Images were obtained at 32-s intervals during the observing period; each frame consists of a 128 × 128 grid of pixels, with an image scale of 3.9 arcsec per pixel. Both subsets were reduced in the same way with a consistently maintained normalization so that the effects of the anticipated seeing degradation in the afternoon could be studied by comparing the strengths of the oscillations as well as the strengths of the background noise.

Comparing the power spectra shown in Fig. 4-2 makes it immediately obvious that the ridges extend to higher ℓ values for the morning half relative to the afternoon half. In the morning half the ridges extend clearly to about $\ell = 600$ while in the afternoon half they extend clearly only to about $\ell =$

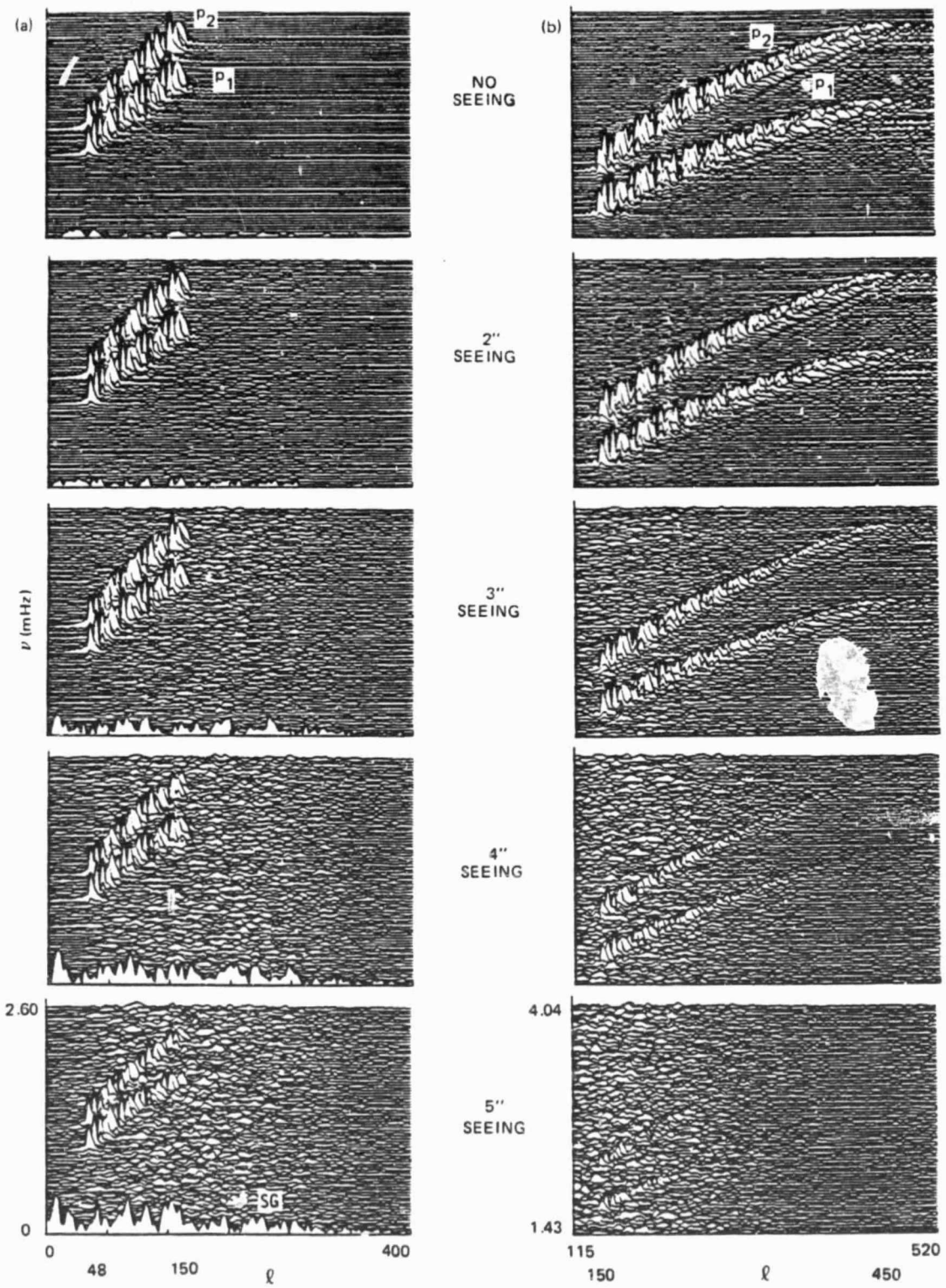

Fig. 4–1. Power spectra in frequency ν and degree ℓ obtained from numerical simulations of how solar oscillations appear when observed through a turbulent atmosphere: (a) On the left are shown power spectra of simulations carried out with p_1 and p_2 modes of intermediate degree ℓ (ranging from 48 to 150) as the quality of the seeing worsens, varying from no seeing distortions (top panel) to poor seeing conditions with typical 5 arcsec displacements (bottom panel); (b) On the right are shown simulations of high-degree modes (with ℓ ranging from 150 to 450) for a similar variety of seeing conditions.

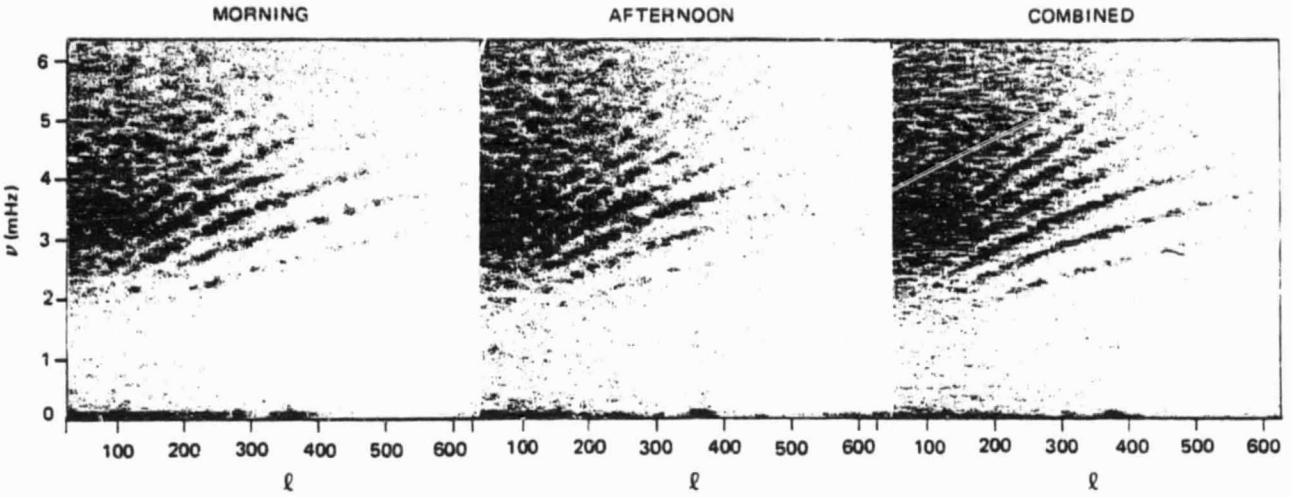

Fig. 4–2. Power spectra of solar oscillations obtained from Doppler observations carried out at Mt. Wilson using magneto-optical resonance line filter. Spectrum obtained under conditions of good seeing in the morning may be contrasted to that obtained with worsening seeing conditions in the afternoon; spectrum of the combined data set is on the right.

450. The afternoon seeing at Mt. Wilson is typically about 4 arcsec while $\ell = 450$ corresponds to a wavelength of about 13 arcsec, so it appears that seeing distortion at a scale of perhaps one-third the wavelength may be sufficient to broaden the ridges until they effectively disappear. The second prediction, that background power is increased by mixing from parts of the ℓ-ν diagram where the solar power is high, was tested by calculating the average power in extended regions of the ℓ-ν diagram for the morning and afternoon runs. It was found that for high ℓ (in the interval 100 to 300) the ratio of measured power on either side of the 5-minute band of peak power to that within the band increased from morning to afternoon by a factor of about two to three. For even higher ℓ ($300 \lesssim \ell \lesssim 500$), the same ratio increased by a factor of up to 4. These results are consistent with predictions and indicate that ground-based measurements of oscillatory power in regions of the ℓ-ν plane with relatively low-solar power can be seriously compromised by seeing effects. These would be particularly deleterious for long-period oscillations because of variable seeing over the course of the day.

B. The Problem of Data Gaps

Were we to employ Fourier analysis on an uninterrupted, infinitely long string of observations of solar oscillations, we could be quite confident that the resultant power spectrum represented the Sun, within the constraints imposed by finite-mode lifetimes and noise introduced by the Sun itself. However, any practical ground-based observation will be of limited duration and will usually contain gaps produced by the setting of the Sun, interruptions by clouds, equipment failures, etc. The distortion of the true spectrum produced by these limitations can fortunately be calculated precisely for any specified pattern of gaps. We have carried out such calculations as part of this study, and discuss them in detail in Appendix B. In that appendix we also report on investigations we have made into the use of mathematical techniques to repair the damage caused by gaps in the data. Here we very briefly summarize the results of the work.

A finite data string causes the individual lines of the oscillation spectrum of the Sun to be broadened by the amount $1/T$, where T is the total duration of the observation string. It also produces noise in the data, including spurious sidelobes caused by regularities in the sequence of gaps in the string, such as those due to a day-night cycle. Numerical calculations, using realistic simulated data with various levels of noise and various patterns of gaps, have shown that with data of sufficient signal-to-noise ratio, and with gaps amounting to less than 20% of the total observing time (that is, with an 80% duty cycle), almost perfect reconstructions can be obtained using maximum entropy techniques to fill the gaps. At a 60% duty cycle there was a slight degradation in the ability to detect very low amplitude peaks, while at 30% duty cycle only the very strongest peaks were recoverable and sidelobes often could not be distinguished from true peaks. This implies that, at least for low- and intermediate-degree observations where seeing is not a fatal problem, ground-based observations can be very useful, provided a duty cycle of 60% to 80% can be maintained.

In principle, a long data string with a high duty cycle and relative freedom from periodic interruptions could be achieved

Appendix A

Numerical Simulations of the Impact of Atmospheric Turbulence

We assess here the effects of atmospheric seeing upon observations of 5-minute oscillations carried out from the ground. This will help to provide a baseline estimate of the scientific benefits that would accrue if one were able to observe the same oscillations from a space observatory unfettered by seeing effects. Such an assessment is not a simple undertaking, for there are wide variations in the seeing experienced at a given observing site and there are equally great changes between different sites. More importantly, seeing produces image distortions that are often truly nonlinear in character, with light travel paths crossing and even focusing onto caustics. Further, the reliable modeling of atmospheric seeing shares the intrinsic difficulties of turbulence theory itself: Both depend critically upon understanding and describing the highly nonlinear dynamics of the atmosphere.

A. Simulated Velocity Fields for Oscillations and Steady Flows

We have constructed synthetic Doppler velocity data sets involving two spatial dimensions and time that would result on the Sun if about 100 modes of oscillation (with distinctive frequencies ν and spherical degrees ℓ) were superimposed upon a persistent background velocity field attributable to supergranulation and mesogranulation. Although on the order of 10^7 modes of oscillation are actually superimposed on the real Sun, our 100 or so modes will serve to sample a fairly broad range of ν and ℓ and thus to identify which modes are affected most severely by the seeing. Therefore, in our high-ℓ simulations we will choose oscillation modes that serve to populate the p_1 and p_2 ridges in power and span ℓ values from 150 to 450 in increments of 6. In the corresponding intermediate-degree simulations, the ℓ values for the sampling modes range from about 50 to 150.

As sketched in Fig. A-1, the Doppler velocities (with suitable geometric projection taken into account) are evaluated for each time interval on a regular two-dimensional spatial grid composed of 256 × 32 elements or pixels in the plane of the sky, with each pixel covering an area of 7″ × 7″. Such a relatively long but narrow sampling window, covering much of the solar diameter along the equator, is appropriate for observing oscillation modes (with azimuthal order m equal to spherical degree ℓ) that can probe the dynamics of giant cells and of differential rotation in the convection zone. Each oscillation mode was assigned a velocity amplitude of 1 m s^{-1} and the phase was random; the persistent background flows possessed vertical velocities with a spatial rms of 50 m s^{-1} and horizontal velocities with an rms of 300 m s^{-1}. The Doppler velocities are evaluated over the spatial sampling window for 512 successive time intervals, each separated by 60 s from the former. Each simulation thus spans about 8.5 hours, comparable to what is typically achievable on a given day from a midlatitude ground observatory.

B. Modeling the Seeing Distortion

The atmospheric turbulence will lead to differential image motion, blurring, and distortion across the field of view in the sky. Theory and experiment concerning such optical turbu-

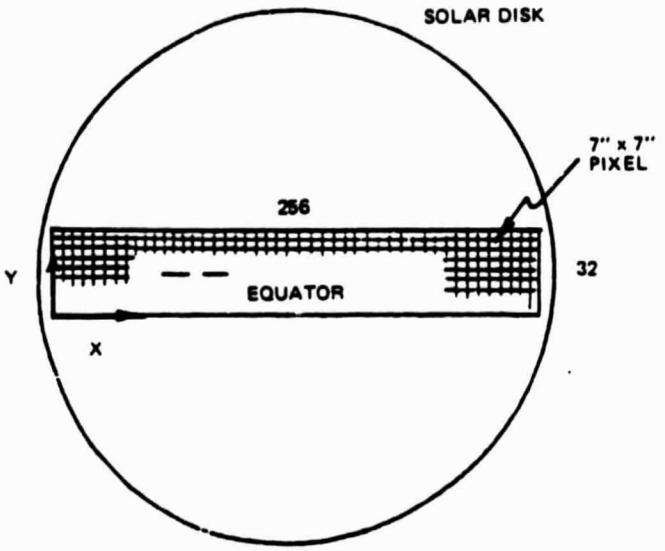

Fig. A–1. Sampling grid 256 × 32 pixels on the solar disk used in simulation of atmospheric seeing effects on observations of solar oscillations.

lence have led to a broad and competent literature which seeks to explain the spectral characteristics of atmospheric seeing and its impact on astronomical observations. We shall not review here the details of the modulation transfer functions, index-of-refraction structure parameters, or transverse coherence links that are the necessary tools of that subject. Rather, we will turn directly to the predictions of typical image displacements that can be expected, with these expressed as Fourier spectra in the temporal and spatial frequency domains.

We will simulate the effects of seeing by evaluating at any given instant in time an array of image displacements across the field of view. The Doppler velocities as previously calculated on the solar disk are then "observed" through such a seeing displacement array. This serves to displace each image element in a particular spatial direction by a specified fraction or multiple of a pixel. The observed Doppler velocity field at a given pixel may thus involve fractional contributions from many nearby pixels.

The instantaneous two-dimensional image displacement arrays are constructed by inverse Fourier transforms of a two-dimensional spatial power spectrum that possesses a Kolmogorov $k_h^{-5/3}$ decrease at high horizontal wave numbers k_h, preceded by a relatively flat plateau between a range of lower wave numbers. The plateau at low k_h corresponds to the large scales of turbulence that are dynamically driven; a turbulent cascade of energy to higher wave numbers produces the Kolmogorov inertial range. Accurate telescope guiding is assumed to compensate for the seeing displacements of very large spatial scale (or small k_h); consequently, the power in the transforms is assumed to vanish as k_h goes to zero. Added to the power spectrum is proportional Gaussian noise at all wave numbers; the specified phases for the transforms are obtained from uniformly distributed noise. We can consider a variety of seeing conditions by varying the upper and lower cutoff wave numbers for the plateau in the power spectrum. For convenience, we will generally specify the quality of the seeing by just referring to the rms average spatial displacement that results from a given class of these power spectra.

The seeing displacements vary rapidly in time compared to our once-per-60-s sampling of the Doppler velocities. As in the spatial domain, the representative temporal power spectrum of seeing displacements possesses a plateau followed by a Kolmogorov decrease with increasing frequency. Since the transition is already achieved at periods of only a few seconds, seeing displacement arrays separated in time by more than about 5 s would show almost no correlation. We have exploited this property in our simulations by constructing a large number (64 or greater) of spatial displacement arrays and then by proceeding to randomly select one of these to apply the seeing displacements at any given instant in time. We further can estimate the benefits of long exposures by applying a sequence of image displacements to a given velocity realization.

Our simulations in many ways represent optimal estimates of what can be done from the ground, for we have omitted all explicit effects of noise introduced by instrumentation to measure the Doppler signal and have not concerned ourselves with how fluctuations in the transmission of intensities in the atmosphere would influence the determination of Doppler velocities from spectral lines. These are all quite subtle issues that depend in detail upon the Doppler analyzer that is being used.

C. Analyzing the Observations

The velocity fields that have been subjected to seeing distortions are then analyzed to determine how the power in the oscillations may have been redistributed in both frequency and wave number. Any given data set consists of 512 time samples of 256 × 32 spatial arrays. In order to isolate those oscillation modes that travel along the equator from other signals, we will suitably average the Doppler velocities in the shorter spatial dimension (shown as y in Fig. A-1), thereby obtaining a data array in the remaining spatial dimension (x) and in time (t). Such an array is then Fourier transformed to construct two-dimensional power spectra in the horizontal wave number k_h (or spherical degree ℓ) and frequency ν. Corrections are made for the effects of viewing a spherical surface with a rectangular array of evenly spaced pixels. Finally, detailed comparison is made of the resultant power spectra obtained with different qualities of seeing.

D. Results of Seeing Simulations

The results of atmospheric seeing are most conveniently illustrated in contour plots of the "observed" power levels as functions of frequency ν and horizontal degree ℓ. Such illustrations are given in Fig. A-2 for 2 and 3 arcsec seeing and in Fig. A-3 for 4 and 5 arcsec seeing. Both figures deal with oscillations of high ℓ, ranging from 150 to 450. The power spectra shown in the upper panels (a) are based on one single short exposure per Doppler measurement; here the steady background velocity fields of supergranulation (SG) have been omitted. In contrast, the spectra shown in the middle panels (b) include the effects of those persistent velocities. Finally, the spectra in the lower panels (c) display the benefits of using long exposures per measurement of the combined oscillatory and steady velocities; these exposures average over 4 seeing realizations for each measurement. The 2″ seeing shown in (a) has little effect on the ridge structures, whereas 3″ seeing has already diminished the power levels in the ridges at the higher ℓ values. This tendency is accentuated with 4″ seeing, and 5″ seeing yields very feeble and severely shortened ridges. The inclusion of the supergranular velocity fields has an effect that is increasingly dramatic as the seeing degrades. Whereas the power spectrum in panel (b) with 2″ seeing and a short exposure just shows a mild increase in the noise level between the ridges, the adjacent panel with 3″ seeing shows a prominent increase in the choppy background of power. Going to the companion spectra with 4″ seeing shows that the ridges in power are almost becoming obliterated by the background, as they indeed are with 5″ seeing. The longer exposures in panels (c) help to diminish the background choppiness, yielding ridges that are now somewhat discernible with 4″ seeing but not usefully so with 5″ seeing.

These seeing simulations of high-ℓ oscillations, with ℓ ranging from 150 to 450, reveal that atmospheric turbulence can severely degrade the Doppler velocity data and that the higher ℓ values are affected the most seriously. The signal-to-noise ratio in these (ℓ, ν) power spectra is influenced by seeing in two ways. First, seeing distortions of the oscillation wave fronts cause some of the power to be moved away from their appropriate (ℓ, ν) values. This process is more vigorous for oscillations with the shorter horizontal wavelengths (or greater ℓ values). Thus the ridges in power are preferentially obliterated at their high ℓ values. Just as damaging is the fact that random image displacements convert steady velocity signals from the strong supergranular flows into apparently time-varying signals. Therefore power is partially redistributed from what should be zero frequency to a broad range of frequencies, causing the prominent noisy background that appears in the power spectra as the seeing gets worse. The impact of the atmospheric turbulence is thus twofold: Not only do the ridges shrink in height, but the background due to persistent flows also rises up to further decrease the signal-to-noise ratio. It is this ratio that is critical to all of the applications of inverse theory to deduce the interior dynamics and structure. Namely, a wide selection of frequencies for the oscillation modes must be measured as precisely as possible, and the accuracy of such determinations depends sensitively on how well the power attributable to the oscillations can be isolated from the background. Using long exposures helps to somewhat mitigate the effects from supergranulation, but with 4″ seeing there is little useful oscillatory signal left for ℓ values greater than about 300. Further, at ℓ values around 200, the signal-to-noise ratio in both the p_1 and p_2 ridges typically decreases by about a factor of 3 in going from 2″ to 3″ seeing, and a further factor of about 3 in going to 4″ seeing. With 5″ seeing there is little signal at $\ell = 200$ that survives over the background.

We estimate that what we designate as 2″ seeing corresponds to superb seeing conditions rarely encountered at most observatories, while 3″ seeing is more typical of a day of consistently good seeing, and 4″ seeing represents the worsening conditions often encountered under turbulent conditions. These numbers are not intended to be absolute, for we can adjust the plateau in the original input power spectra for the image displacements and thus somewhat worsen or improve the final (ℓ, ν) power diagrams shown here. However, the changes are systematic and gradual across the matrix of seeing that we have sampled, and thus we have chosen parameters for the illustrations here that appear fairly representative of atmospheric conditions.

The seeing simulations with intermediate ℓ oscillations, with ℓ ranging from 48 to 150 (Fig. A-4), show that modes with large horizontal wavelengths are not badly affected by the seeing until the seeing deteriorates to rms image displacements of about 4″ or 5″. These two seeing conditions are displayed in Fig. A-4, using a layout similar to the earlier figures except that the range of displayed frequencies ν and spherical degrees ℓ now both extend to zero values. The upper panels (a) again present power spectra obtained with short exposures while omitting supergranulation, while those in (b) include effects of persistent velocities that yield a very noisy background. Going to longer exposures in (c) serves to reduce that background somewhat. The jagged structures in power at $\nu = 0$ in panels (b) and (c) show the distribution with ℓ of power in the persistent velocities (after averaging across the shorter dimension y of the observing window). The noisy background at other frequencies reflects the range in ℓ present in such supergranulation. From these intermediate degree simulations we conclude that the signal-to-noise ratio in the vicinity of $\ell = 100$ is about a factor of 3 worse with 4″ seeing than it is with 2″ seeing, while that ratio at $\ell = 50$ is only slightly affected by the range of seeing conditions considered here.

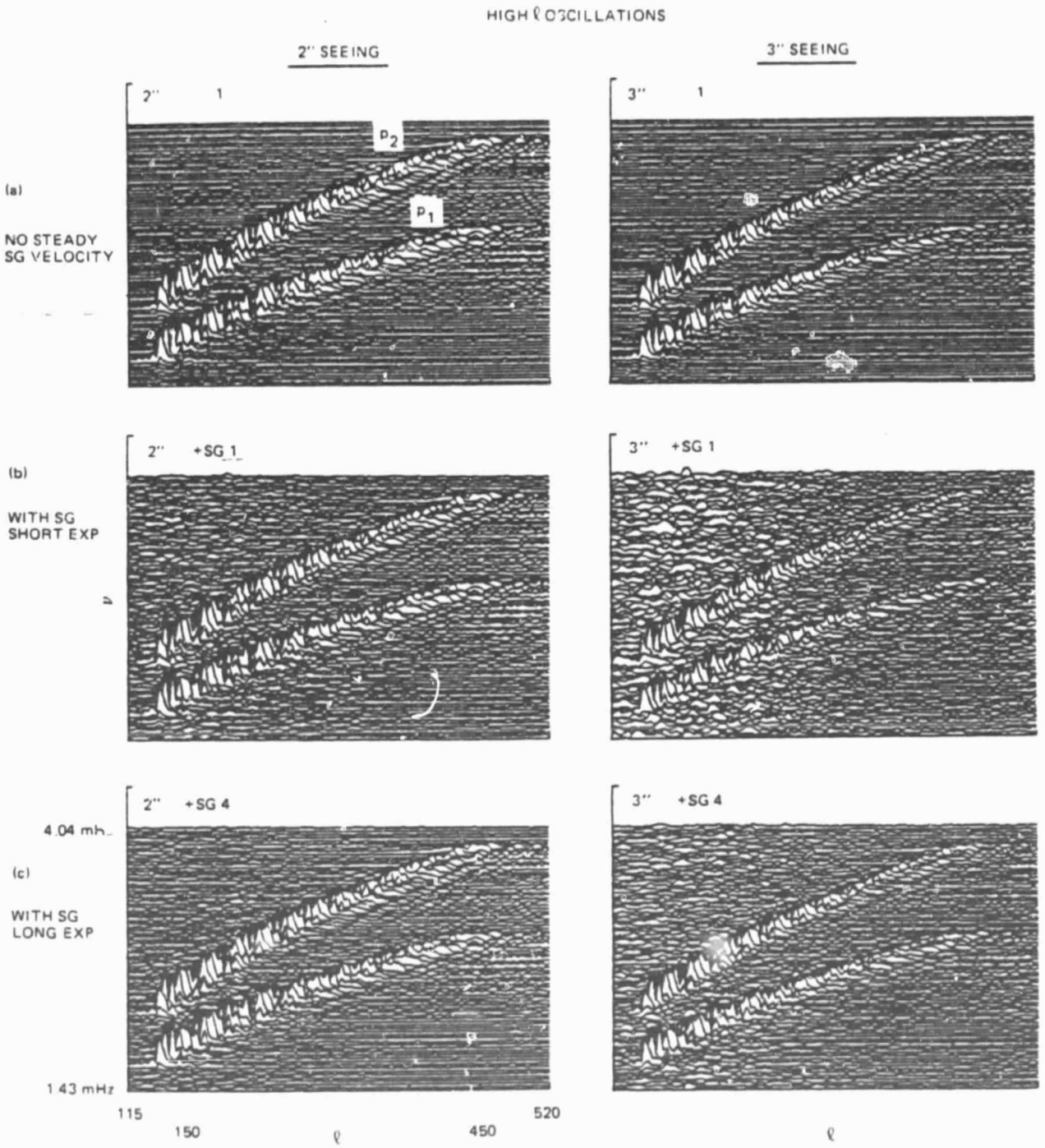

Fig. A–2. Effects of image distortions arising from atmospheric turbulence upon observations of high ℓ oscillation modes. Shown are power spectra in perspective views as functions of ℓ and ν. Considered are p_1 and p_2 modes with ℓ ranging from 150 to 450. Panels (a) show power spectra of oscillations observed through seeing models possessing typical rms spatial displacements of 2" and 3". Panels (b) superpose persistent velocity fields of supergranulation (SG) upon those of the oscillations and then observe the combined Doppler velocities under both 2" and 3" seeing conditions. Panels (c) show power spectra in which the background noise is decreased by having used long exposures for each measurement of velocities.

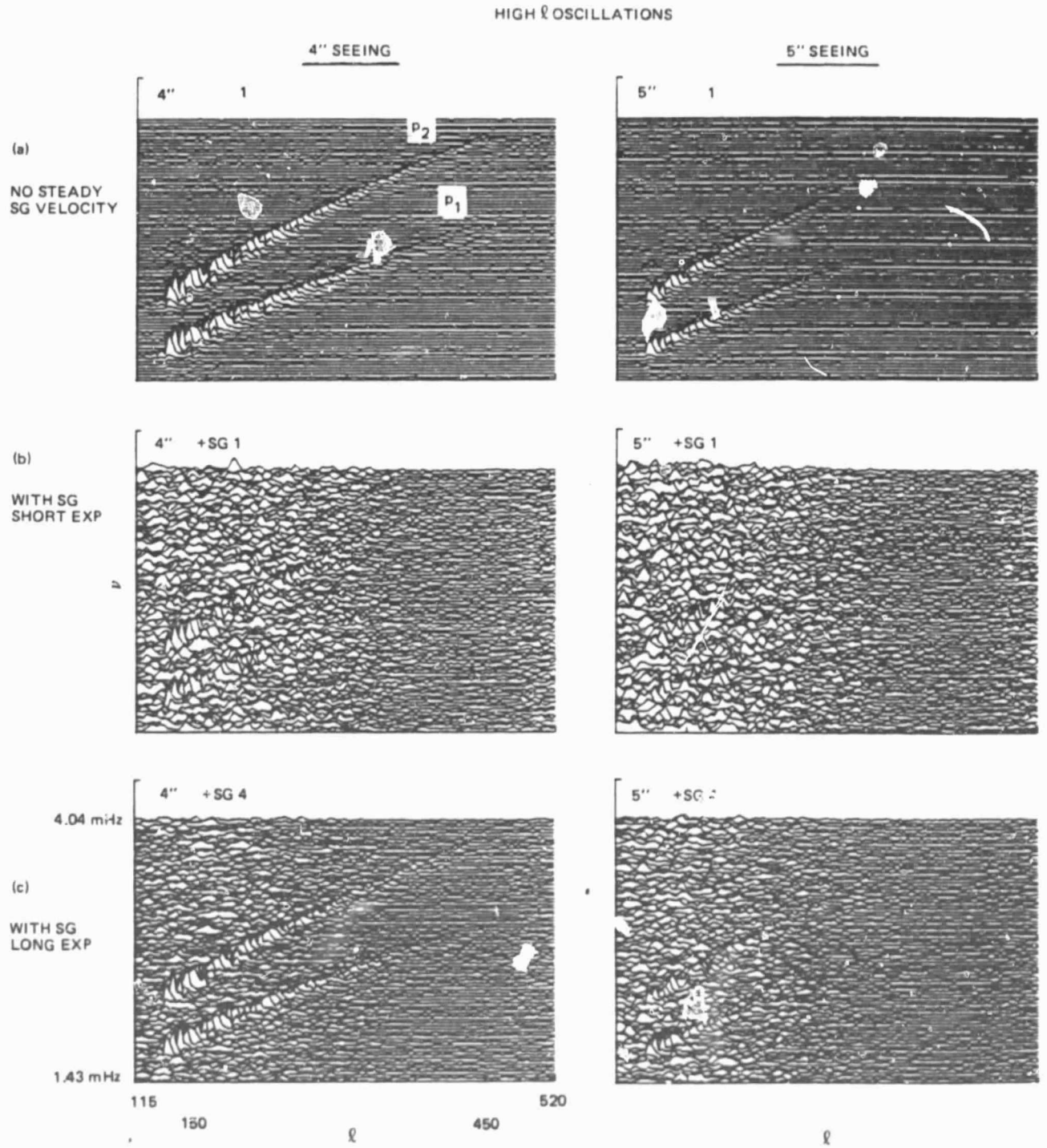

Fig. A–3. As in Fig. A–2, but now considering how 4" and 5" seeing conditions have changed the power spectra of the high ℓ oscillations.

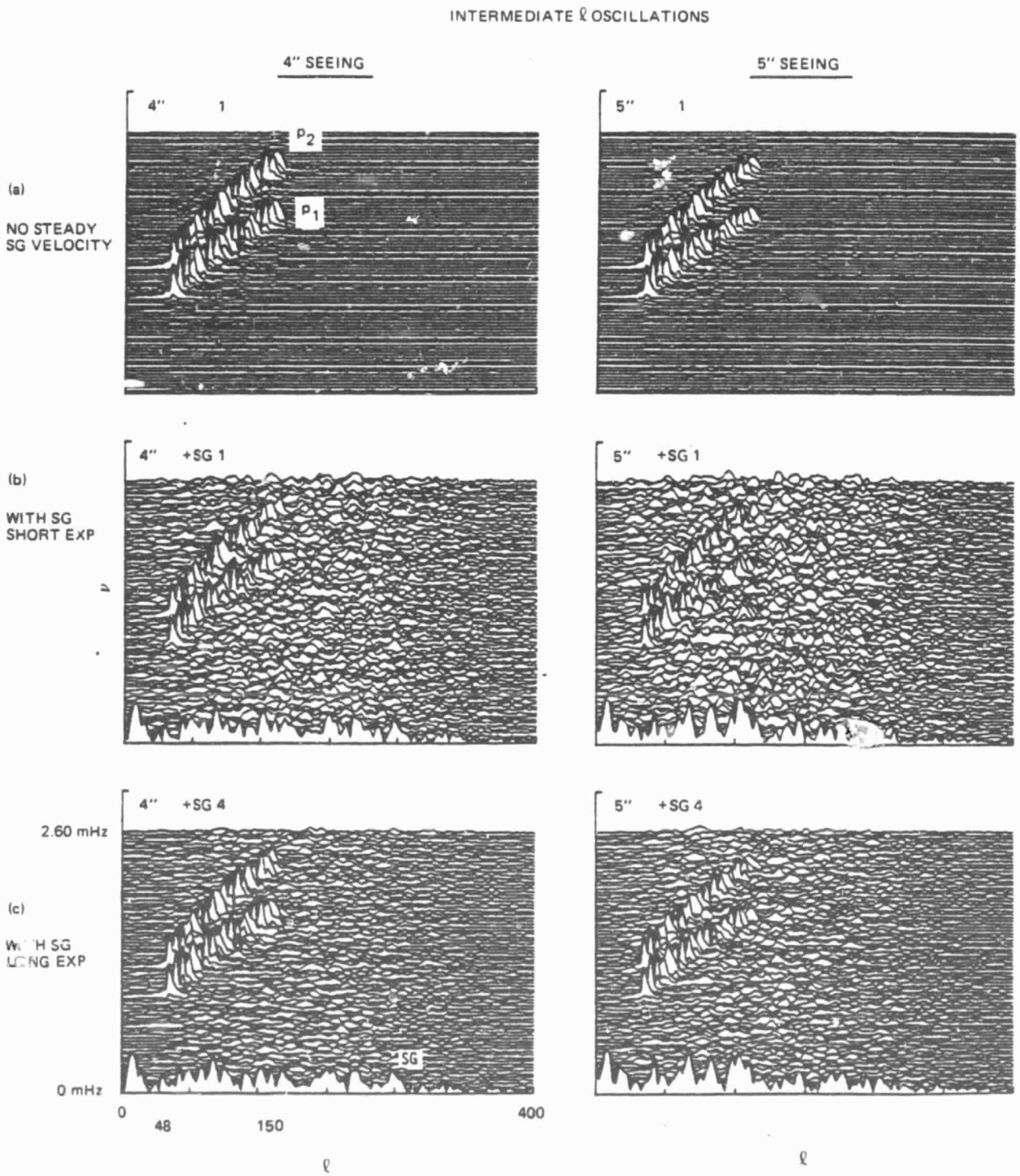

Fig. A–4. As in Fig. A–2, but showing power spectra for the intermediate ℓ simulations using modes p_1 and p_2 with ℓ values ranging from 48 to 150. Here effects of 4" and 5" seeing conditions are displayed.